Small UAV Airborne Electric Field Measurements

Yongming Zhang, Eric Duff, Adam Agundes, Beau Yeik

QUASAR Federal Systems, Inc.
San Diego, USA
yongming@quasarfs.com

Kenneth L. Cummins

Dept. of Atmospheric Sciences
University of Arizona
Tucson, USA

Abstract— **QUASAR Federal Systems (QFS) has validated the technical and logistical elements required to use small unmanned aerial vehicles as low-cost and maneuverable platforms to measure electric fields in and around storm systems. Small electric field sensors are based on an AC electrical potential sensor called the "RVS". Two alternative implementations produce a modulated signal characteristic of the electric field. In one, the motion of the airplane modulates the local fields into an AC signal. In the other, the RVS is mounted on the cone of a small speaker. Driving the speaker moves the RVS within the local fields, generating a signal at the drive frequency.**

Multiple UAVs were built and instrumented, and field tests were conducted during storms in New Mexico and at Kennedy Space Center (KSC). These tests demonstrated the feasibility of deploying low cost, small UAVs to measure DC E-field in or near a storm.

Keywords—electric field measurement; airborne; small UAV; storm; lightning detection

I. Introduction

To better understand storm electrification and its discharge through lightning, it is important to measure the local electric field simultaneously at multiple locations within and outside a storm. Previous in-storm electric-field data collections have employed sensors mounted in fixed-wing aircraft or balloons, coupled with ground-based observatories. However, aircraft require costly customization for storm measurements and are expensive to operate and maintain, while balloons only allow one pass through a cloud, collecting data on a mostly vertical, uncontrolled path. QUASAR Federal Systems (QFS) has defined an alternate path - instrumenting a low cost, small unmanned aerial vehicle (SUAV) that can be launched and landed with a minimum of infrastructure. This paper discusses novel, small, lightweight sensors suitable for such applications, appropriate SUAVs, and the logistical requirements to perform such operations.

II. Sensors

A. DC E-field Sensors

The current generation of QFS's E-field sensors is built upon a new class of compact, lightweight electrical potential sensor product (called the Remote Voltage Sensor, or RVS, see Fig. 1) developed by QFS through a previous NASA program (NASA, 2006). Its specifications are:

Sensor Dimensions: 18 mm diameter, 5 mm height
Bias Current: +/- 75 µA
Transfer Function: 0.04 at 1 Hz and above
Frequency band: 0.2 Hz to 50 kHz
Output Noise (typical): 20µV/rtHz@1Hz, 4µV/rtHz @10Hz
DC Offset: < 3 mV

Fig. 1. QFS RVS Sensor.

These are highly sensitive and robust standard products that measure the local potential at the sensor with respect to a common reference point, which on this program was generally the conductive skin of the aircraft. If a difference is taken between two sensors, the contributions of the grounding point potentials cancel, so the result is the potential difference between the two sensor positions.

However, the sensors are AC sensors, and were not developed for this program's DC-field measurement application, so additional innovation was required. It was necessary to modulate the DC signal into a frequency band acceptable to the sensor. A traditional field mill accomplishes

this by means of a rotating grounded shutter, which is too big, fragile, and heavy to be optimal for a small UAV. Two alternative approaches were developed and used on this program, producing two types of usable sensors that are suitable for SUAVs: "Aircraft movement sensors" and "Speaker sensors."

B. Aircraft Movement Sensor

Aircraft are constantly in motion. Even when they are flying "straight and level", there are continual small adjustments. Moreover, intentional motions can easily be commanded from the flight controls. If pairs of sensors are mounted on different portions of the airframe, aircraft motion will move them differently through an external field, resulting in different potential changes for each sensor. Even when mounted on a conducting, and hence isopotential, plane body, the way that the potential lines bend in the vicinity of the sensor will vary with plane orientation. Thus, a signal (such as a vertical DC E-Field) will be present in the difference between the sensors' measured potentials at the frequency of the aircraft movement. This signal can be correlated with an independent measure of aircraft motion to produce field measurement. This program tried two independent measures of aircraft motion: an accelerometer and a gyroscope. Fig. 2 shows the mounting of two pairs of sensors, one pair mounted on the top surface of the plane along the y-axis (called y sensor pair) and one pair mounted at the bottom surface along the x-axis (also called x sensor pair). To avoid the impact of charged rain drops on the field measurement, we moved the x sensor pair from the top surface to the bottom (as shown in Fig. 2) in 2013. The y-axis sensor utilizes the plane pitch motion to make the DC measurement, while the x-axis sensor utilizes the roll motion to make the DC measurement. The sensors can be calibrated in a pair of big parallel plates, after mounting them on the plane.

Fig. 3 shows the results of a ground-based validation of the aircraft movement sensor at Langmuir Laboratory in New Mexico. The plane was suspended from a tripod and allowed to sway in the wind during a time period when a storm passed overhead. A nearby field mill instrument measured the vertical electric field. The data from the RVS sensors and an accelerometer on board were post-processed to produce the DC field measurements shown in the figure. The fields measured by the "aircraft movement sensors" are in good agreement with the field mill data, especially in the time window after 10:29 p.m. The measurement from the y-pair has lower noise than that from the x-pair. The sensor x-pair or y-pair provide independent measurement of vertical E-field.

Note that external electric field measurement using the aircraft movement sensors is inherently insensitive to charging of the airframe. Charging/discharging that happens to correlate with the aircraft movement will appear as external field, but any fields generated by static charge on the airframe will move with the airframe and therefore produce no signal. This is strictly true if the airframe is isolated in space. But if there is mobile charge in the vicinity that moves in response to the movement of a charged airframe, then that moving charge would cause a correlated signal. But since meteorological distance scales are vastly larger than the airframe, a significant mobile charge will not be perturbed appreciably by small airframe

movements. This may not be true in a ground-based calibration facility in which the external field is produced by conductive surfaces near the aircraft.

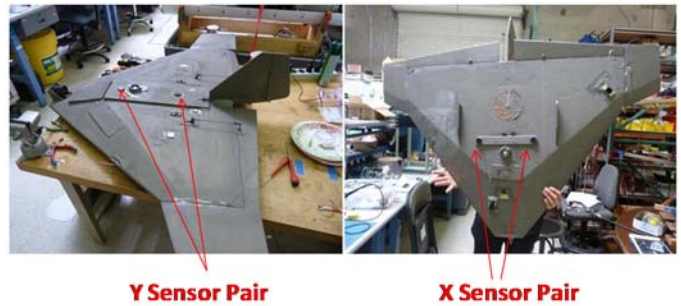**Y Sensor Pair**   **X Sensor Pair**
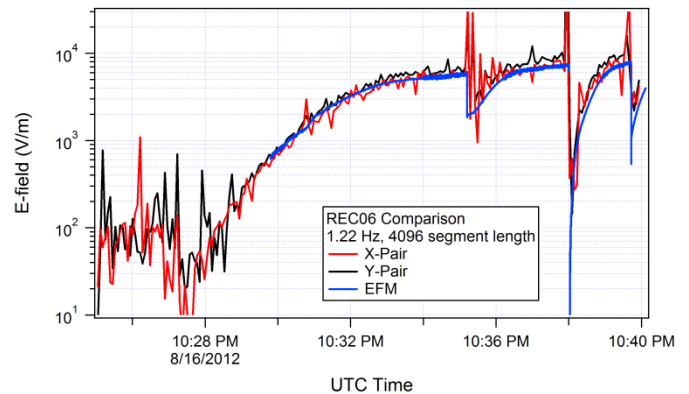
Fig. 2. Pictures of aircraft movement sensors.

Fig. 3. Ground-based validation of the aircraft movement sensor. The red curve is the DC field measured by the x-pair sensor, and black-curve is the field measured by the y-pair sensor. The blue curve is the field measured by a DC field mill nearby.

C. Speaker Sensor

An alternative to modulating the potential of the sensor using the movement of the plane is to actively drive sensor position with respect to the plane. This is accomplished using the system depicted in Fig. 4. In this system, the RVS is mounted on the cone of a small speaker, which moves its position in space. If there is electric field normal to the RVS surface, that motion will produce a change of electric potential detected by the RVS. In our current embodiment, we drive the speaker at 41 Hz. This frequency is not optimized, but was chosen for the following reasons:

- It is clear of 60 Hz and other strong noise sources seen on the plane in flight.

- Is relatively slow, allowing the small speaker to drive the mass of the RVS sensor through a significant distance.

The modulation can be sampled by the 24-bit data collection board (mounted inside the payload bay), which is sampled at 1 kHz.
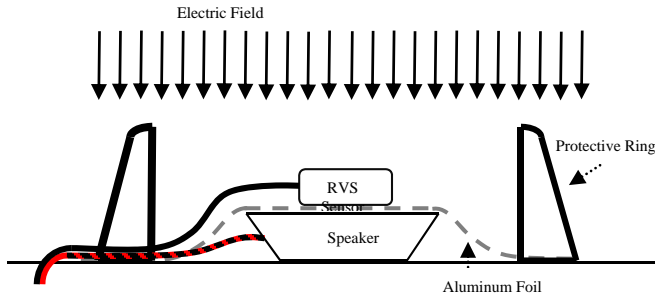
Fig. 4. Speaker sensor photograph and diagram. The protective ring was used as a rain shield to block raindrops during the flight.

It is straightforward to extract from the output of the RVS sensor a signal at 41 Hz, which is proportional to the observed field. However, since the RVS is moving with respect to the aircraft surface, the measured signal is strongly affected by any charging of that surface. Therefore, a pair of speaker sensors must be mounted in similar configurations on the top and bottom of the aircraft. Taking the sum and difference of measured signals allows independent measurement of the external field and the signal generated by the aircraft surface charge.

A ground-based validation of the speaker sensor was conducted in San Diego during a time when only fair weather field variations were available. Fig. 5 shows a comparison of DC-field data measured by the speaker sensor (red curve) with data (black curve) measured simultaneously by a field mill on the ground. They are in good agreement.
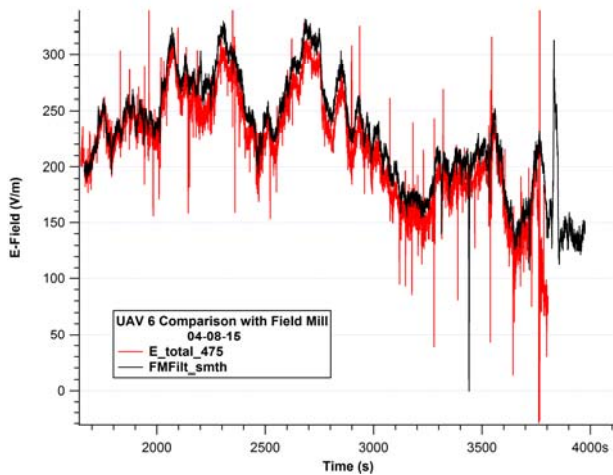

Fig. 5. Ground-based validation of the speaker sensors mounted on a SUAV.

Measurements in a large outdoor calibration facility (Fig. 7) demonstrate good readings at levels exceeding 4 kV per meter, and show good rejection of injected charges on the plane's surface using a pair of sensors - one on top and one at the bottom of the plane. There is every reason to expect good performance with much higher fields. In Fig. 6, we show the results of one experiment run, with an applied field at +2 kV/m, +4 kV/m, and -2 kV/m, -4 kV/m. The plane is 1 m above the ground. At the 2 kV/m field, we also applied a ~450 V probe directly to various locations of the plane for between 900 s and 1700 s. We can see that the impact of the charge on the E-field measurement is very small.
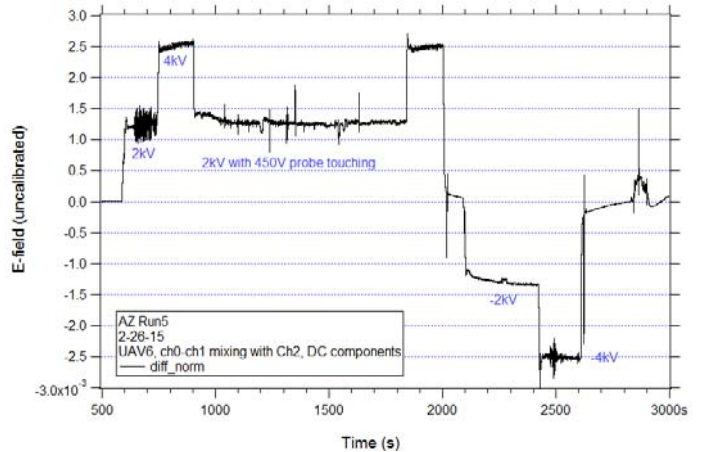

Figure 6. E-field (uncalibrated) measured in a large calibration facility. Two speaker sensors were mounted on a SUAV, one on top (Ch0) and one on the bottom (Ch1). The plot is the mixing product of the (Ch0-Ch1) with the speaker modulating source (Ch2) at 41.5 Hz.

D. Sensor Calibration

Extensive work was conducted to calibrate both sensor types using both a large parallel plate capacitor (1 m spacing, 2 m diameter), and a larger outside facility in Arizona. Additional calibrations were done using small plates attached to the airframe over the sensors and charged to given voltages with respect to the airframe. These calibration plates are in place in the photograph in Fig. 7. Calibration is complicated by inadvertent charging of the airframe and objects in the vicinity. We did eventually develop methods to obtain absolute calibration values of the terms required to produce the speaker sensor data. Less absolute quantitative calibration work was done on the aircraft movement sensors, with the data in Fig. 3 being adjusted by a few fitting constants to match the scale of the field mill results. Once established, those constants can be used until the hardware or configuration is changed.
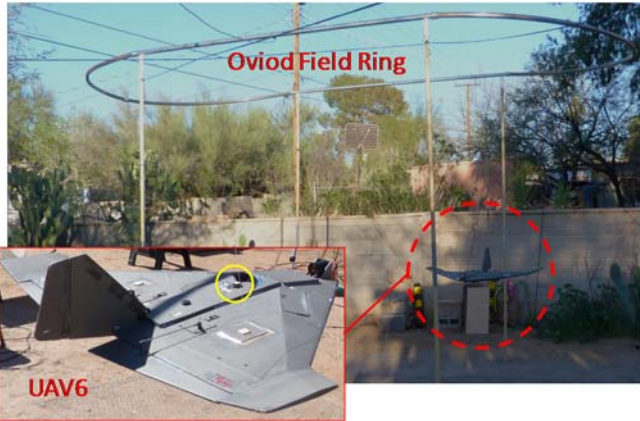
Fig.7. Indoor (upper) and outdoor (lower) calibration facilities. In the lower photo, the upper sensor is marked by a yellow circle.

Extensive work was conducted to measure the stability of the speaker sensors in temperature changes. Significant variations are seen, with sensitivity changing on the order of 10% over a 30 C temperature change. Post-processing with reference to a plane-mounted temperature sensor should reduce this error by at least half. A thin aluminum foil wrapped around the speaker can improve the temperature stability of the speaker and provide a better reference potential.

III. FLIGHT PLATFORM

This program focused on the Spear UAV produced by Co-Operative Engineering Services (CESI), a small company that served as a partner on this program in the production and operation of aircraft. The CESI aircraft was chosen because its construction and performance seemed compatible with program goals. It was also an attempt to straddle the divide between the innovation and low cost of hobbyist technology and the stability and reliability of the much more expensive commercial and military offerings. Over the course of the program, six planes were built and instrumented, all variations of the simple delta wing design (called Spear) shown in Fig. 8. Aircraft were electrically powered for simplicity of operation.

Fig.8. Example Spear aircraft.

Although the performance of each plane was different, in broad summary, flight speeds of 35 to 70 mph proved appropriate for the task. Flight times of 20-30 minutes and a climb limit of a few thousand feet were very marginal, making it necessary to employ balloon launches in some cases. An additional significant challenge was that the aircraft needed to operate across a wide range of altitudes, complicating the choice of motor and propeller.

In order to make it possible to recover the UAV in complex terrain, a transmitter from a commercial pet locating device was added to the planes to locate them using GPS tracking technology.

A. Launch

Depending on the aircraft, the Spear was launched either by hand (limited by weight, only possible for UAVs #5 and 6 during the program) or using a catapult (implemented and tested for UAV #1-4) as shown in Fig. 9. Although both were workable, experience in complex storm logistics environments suggest that simpler is better. Ideal platforms for future campaigns will either be hand launched, or autonomously launched from a runway or catapult.

Fig. 9. Launch catapult and hand launch.

B. Landing

The Spear aircraft was able to land in an open grassy area, if available, or in a net (Fig. 10). The net landings placed much higher demands on the pilot, and involved a higher risk of damaging the aircraft. However, it was the best choice when landing at very high altitude sites. Landing without a net requires a flat grassy area, which was available at KSC but not at Langmuir Lab. Auto landing is feasible in an open area.

Fig. 10. Landing net.

C. Balloon Launch

The Spear aircraft only had battery capacity to climb a few thousand feet. Because electrical activity generally occurs at much higher elevation, capability was developed to loft the Spear under a balloon to high elevation, release it, and let it fly down. When flying level or descending, flight times can be very long. An actual balloon launch is shown in Fig. 11. In flights at Langmuir Lab, the aircraft was released from the balloon at around 20,000 feet above sea level, roughly 10,000 feet above launch point. This height limitation derived from (solvable) communication range issues, and from concerns about the winds pushing the aircraft outside of the controlled airspace in which it was required to operate.

Fig. 11. Balloon launch.

IV. OPERATIONAL LOGISTICS

Operational logistics proved critical to the success of this program. Key elements included:

1. **Airspace and procedural coordination.** At present, operation of UAVs with significant altitude in the US is only permitted in restricted airspace. Use of such airspace often requires significant documentation and review for approval, and careful and constraining coordination with other airspace users. In many cases, the operations team will include a representative of or liaison to a local operating facility.

2. **Lightning safety.** This program's testing inherently involves operations and conditions that may pose a lightning hazard. It is important to have clear safety procedures in place, and may be necessary to have approval from the operating facility for variance from their global policies. This was necessary and achieved when operating at Kennedy Space Center. There should be a specific individual charged with and empowered to interpret and enforce lightning safety rules.

3. **Weather forecasting and now-casting.** When and where to fly requires optimum information about the current weather and likely evolution of that weather. It is essential to have real-time discussions with skilled meteorologists who are familiar with local weather patterns and have access to weather data ranging from networked external sources through the view out the window. Dr. Walt Lyons from FMA Research filled such a role during this project.

4. **System reliability**. Because storms cannot be scheduled, it was essential to develop hardware and procedures that allowed rapid and reliable action whenever desirable weather materialized. In practice, we developed procedures to prepare systems and enter a "10-minute hold", from which we could launch on 10 minutes notice.

5. **Flight situational awareness.** Decisions on where and when to fly must be made in real time, for which it is necessary to understand the spatial and temporal evolution of the storm and of the flight of the aircraft. NASA Marshall Space Flight Center adapted their real time mission management (RTMM) tool for our purposes (example outputs are shown in Fig. 12 and 13). As integrated, this visual tool displays in real time on a scalable local map the airspace and locally-defined boundaries, the plane position, and weather data from a variety of sources, including radar and lightning data. The tool ingests the plane telemetry data and other weather data, and displays them in near real-time via the Internet. Seeing the plane's path and real-time weather on a common display proved invaluable. The tool was also used in post-analysis.

V. SYSTEM/CAPABILITY DEMONSTRATIONS

Over the course of this program, over 50 flights were performed as part of eight different flight tests: two at Camp Atterbury in Ohio, two at Langmuir Lab in New Mexico, and four at Kennedy Space Center in Florida. Although no flight had everything working perfectly, in this report we review one example when many elements worked well together. This was a balloon-launch flight that demonstrated the feasibility of using a small UAV to perform airborne E-field measurement near a storm.

This flight took place on 7/31/14 in New Mexico. By late afternoon, widespread convection was present over the western and northern parts of the state, with the Langmuir Laboratory site being just beyond the eastern edge of the significant storms. Significant storms formed over the San Mateo range roughly 20 miles SW of Langmuir, but remained pinned to that range instead of propagating toward the Lab. The long-lived convection produced an extensive anvil cloud (clouds that blow laterally off the top of thunderstorms). This cloud did drift over Langmuir, producing elevated fields and becoming the target of the flight. Although anvil clouds frequently lack the vigorous convection required to generate new charging, they transport charge laterally, substantially extending the high-field footprint and lightning potential of a storm.

Radar reflectivity and the LMA+NLDN lightning activity in the 5 minutes prior to launch are shown below in Fig. 12. These images are from the improved RTMM tool. The anvil cloud is the large green region extending from the active lightning areas in the south and west (red symbols) to cover the Langmuir Labs flight box at right of center.
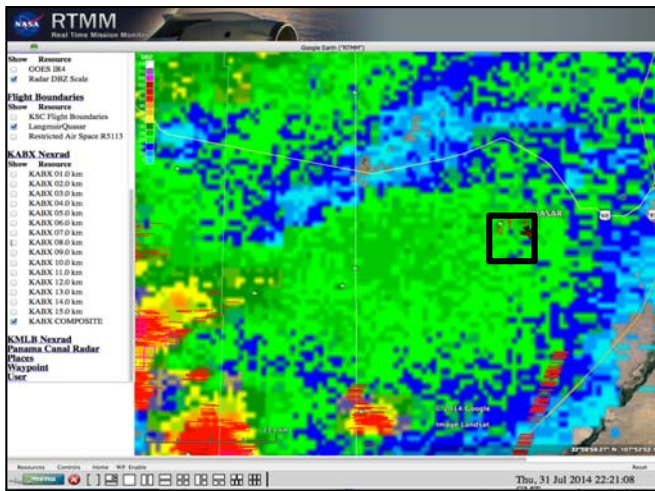
Fig. 12. Composite radar reflectivity. The square box is the flight box.

Fig. 13 shows a map of the flight and a plot of the parameters measured. The airborne E-field was measured by a plane movement sensor mounted at the bottom of the plane, and calculated together with the roll data measured by an accelerometer.

During balloon-assisted ascent, the temperature dropped from 18 C to -6C, and video cameras mounted in the balloon chain showed falling snow/ice particles; frozen precipitation (Graupel) was observed on top of the plane. In this flight, the plane was released from the balloon at around 10:13:20. It dropped from an altitude of 3400 m to about 3000 m. The plane then leveled in straight flight at a temperature of around -6C. Temperature changes associated with altitude are shown in Fig. 13. There is a temperature dip at 10:21, which is the same time the maximum E-field (+18 kV/m) was measured. During the time period of 10:20:00 to 10:23:30, the airborne E-field data suggest spatial field variations in the anvil cloud following 10:20:00. The on-board video also shows that the plane came out of the cloud boundary, and passed over a lower cloud boundary after 10:20:00.
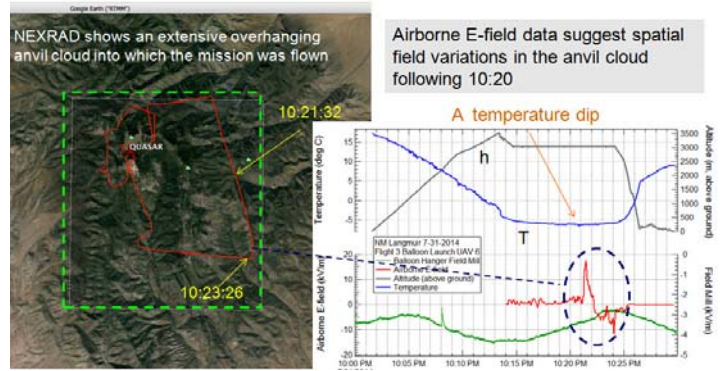

Fig. 13. Left: flight path (red) and the flight box (green). Right: flight altitude (black curve) above ground level, and measured E-field (red curve) and ambient temperature (blue curve). The DC E-field measured by a field mill at the balloon hanger was also shown in the right graph (green curve).

Because of airspace and procedural limitations, flights at Kennedy Space Center were all ground launched with cruising elevations only a few thousand feet above ground level. Fig. 14 below shows an RTMM image of a flight that pursued a high radar reflectivity region indicated by the red tint produced by a semi-transparent composite reflectivity image of areas exceeding 45 dBz.
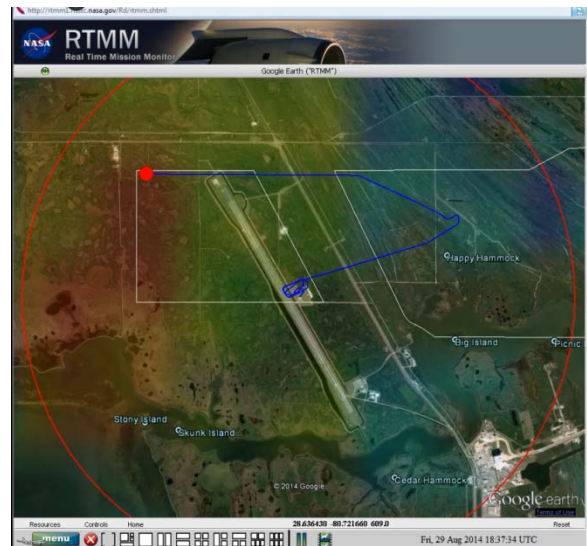

Fig. 14. In-process flight path for a flight (August 29, 2014) at Kennedy Space Center under a high-reflectivity region (tinted red.)

VI. CONCLUSIONS

This program successfully demonstrated capabilities required to use small SUAVs to measure electric field in and around electrified storms. Advances were made in small, compact, lightweight electric field sensors suitable for SUAVs, the flight platform itself, and also in the logistical capability to make it all work. Unfortunately development in all those areas proceeded in parallel so that the sensor technology did not reach its current level of maturity until the end of the flight tests. However, while improvements can be made in all areas, future work should be able to focus on acquiring scientifically meaningful data from storms.

VIII. REFERENCES

Hibbs, A. D., Y. Zhang, and L. J. Burnett (2009), Electric Field Sensing: Measurements and Applications, presented at the Military Sensing Symposium, Battlespace Acoustic and Magnetic Sensors Meeting, Laurel MD.

Mo, Q., R. Feind, F. Kopp, and A. Detwiler A (1999), Improved electric field measurements with the T-28 armored research airplane J. Geophys. Res., 104, D20.

NASA Phase II SBIR Project Multi-pupose Electric Potential Sensor for Spacecraft Applications, completed 12/20/2006

Smith P., Report of the October 2006 Storm Penetrating Aircraft Workshop (2007), Prepared for the National Science Foundation, SDSMT/IAS/R07-01.